Biochemical and Biophysical Research Communications 522 (2020) 585–591

Contents lists available at ScienceDirect

Biochemical and Biophysical Research Communications

journal homepage: www.elsevier.com/locate/ybbrc

Crystal structure of the reactive intermediate/imine deaminase A homolog from the Antarctic bacterium *Psychrobacter* sp. PAMC 21119

Sunghark Kwon [a, 1], Chang Woo Lee [b, 1], Hye Yeon Koh [b], Hyun Park [c, ***], Jun Hyuck Lee [b, d, **], Hyun Ho Park [a, *]

[a] College of Pharmacy, Chung-Ang University, Dongjak-gu, Seoul, 06974, Republic of Korea
[b] Unit of Research for Practical Application, Korea Polar Research Institute, Incheon, 21990, Republic of Korea
[c] Division of Biotechnology, College of Life Sciences and Biotechnology, Korea University, Seoul, 02841, Republic of Korea
[d] Department of Polar Sciences, University of Science and Technology, Incheon, 21990, Republic of Korea

ARTICLE INFO

Article history:
Received 12 November 2019
Accepted 20 November 2019
Available online 27 November 2019

Keywords:
RidA
Deamination
Psychrophile
Antarctic bacterium
Cold-adaptability

ABSTRACT

The RidA subfamily proteins catalyze the deamination reaction of enamine/imine intermediates, which are metabolites of amino acids such as threonine and serine. Numerous structural and functional studies have been conducted on RidA isolated from mesophiles and thermophiles. However, little is known about the structure of the RidA proteins isolated from psychrophiles. In the present study, we elucidated the crystal structure of RidA from the Antarctic bacterium *Psychrobacter* sp. PAMC 21119 (Pp-RidA) at 1.6 Å resolution to identify the structural properties contributing to cold-adaptability. Although the overall structure of Pp-RidA is similar to those of its homologues, it exhibits specific structural arrangements of a loop positioned near the active site, which is assumed to play a role in covering the active site of catalysis. In addition, the surface electrostatic potential of Pp-RidA suggested that it exhibits stronger electrostatic distribution relative to its homologues. Our results provide novel insights into the key determinants of cold-adaptability.

1. Introduction

The YjgF/YER057c/UK114 family proteins catalyze the deamination reaction of enamine/imine compounds by addition of water [1–3]. These compounds can be generated from serine, threonine, and cysteine by serine dehydratase, threonine dehydratase, and cysteine desulfhydrase, respectively [4–6]. These products can form external aldimines by reacting with pyridoxal 5′-phosphate (PLP), which results in the inactivation of PLP-dependent enzymes [7,8]. Since PLP-dependent enzymes are essential to cellular metabolism, the elimination of enamine/imine intermediates via chemical modification is imperative to maintain cellular homeostasis. Hence, the YjgF/YER057c/UK114 family proteins play a vital role in preventing cytotoxicity at the molecular level. This also constitutes the reason for the presence of these proteins in all the three domains– archaea, bacteria, and eukarya.

The YjgF/YER057c/UK114 family was renamed the Rid (reactive intermediate deaminase) family, which reflects its enzymatic function [1,2]. The Rid family is divided into eight subfamilies, RidA and Rid1-7, on the basis of a recent genomic analysis [2]. Among these, RidA is distributed among the three domains [2] and has been well characterized, particularly in bacteria such as *Salmonella enterica* [6,9]. The RidA subfamily proteins have also been characterized biochemically, and have been shown to function as a ribonuclease [10] and an Hsp90-like chaperone [11] as well as a deaminase [1–3]. Additionally, several structures of the RidA proteins have been determined thus far, mostly from mesophilic bacteria such as *Escherichia coli* (PDB code: 1QU9) [12], *Neisseria meningitides* (PDB code: 3KJJ and 3KJK), *Streptococcus pyogenes* (PDB code: 2EWC), *Haemophilus influenzae* (PDB code: 1J7H) [13], *Streptomyces hygroscopicus* (PDB code: 4BPS) [14], *Mycobacterium tuberculosis* (PDB code: 3I7T) [15], and *Bacillus subtilis* (PDB code: 1QD9) [16]. A minority of structures are those from thermophilic and hyperthermophilic bacteria such as *Hungateiclostridium*

* Corresponding author.
** Corresponding author. Unit of Research for Practical Application, Korea Polar Research Institute, Incheon, 21990, Republic of Korea.
*** Corresponding author.
E-mail addresses: hpark@korea.ac.kr (H. Park), junhyucklee@kopri.re.kr (J.H. Lee), xrayleox@cau.ac.kr (H.H. Park).
[1] These authors contributed equally to this work.

https://doi.org/10.1016/j.bbrc.2019.11.139
0006-291X/

thermocellum (PDB code: 1XRG) and *Sulfurisphaera tokodaii* (PDB code: 1X25) [17].

Although the structures of RidA from mesophilic, thermophilic, and hyperthermophilic bacteria have been determined and they have provided useful information to understand their function, biochemical characterization of RidA from psychrophilic bacteria has not yet been well studied. Moreover, the absence of RidA structures from psychrophilic bacteria has rendered a comparative study on RidA relative to temperature difficult. Accordingly, structural studies of cold-adapted RidA may lead to a better understanding of structural properties related to cold-adaptation and provide insight into evolutionary diversification of the RidA subfamily.

In this paper, we report the crystal structure of RidA from the Antarctic bacterium *Psychrobacter* sp. PAMC 21119 (Pp-RidA). The structure of Pp-RidA was compared with those of homologues to identify structural differences, which may impart cold-adaptability to Pp-RidA. In addition, we performed molecular docking simulation with an imine intermediate molecule to better understand the catalytic mechanism at the molecular level. Our results revealed that Pp-RidA has a loop near the active site exhibiting a spatial deviation, which cannot be observed in homologues. Thus, the present study provides structural insights into the enzymatic property of RidA from the psychrophile.

2. Materials and methods

2.1. Cloning, overexpression, and purification

The gene encoding RidA from *Psychrobacter* sp. PAMC 21119 (NCBI entry: WP 010201437.1) [18] was amplified by polymerase chain reaction (PCR). The PCR products were ligated into a pET-28a(+) vector (Novagen, Merck, USA) at the *Nde*I and *Xho*I restriction sites. The recombinant vector was delivered into *Escherichia coli* strain BL21(DE3) for gene expression. The cells were cultured at 37 °C in 4 L of lysogeny broth medium containing 50 μg/mL kanamycin until the optical density at 600 nm reached 0.6. Following this, gene expression was induced by addition of 0.5 mM isopropyl β-D-1-thiogalactopyranoside at 20 °C, and the cells were further cultured overnight. The resulting cells were collected and resuspended in a lysis buffer (50 mM sodium phosphate (pH 8.0), 300 mM sodium chloride, and 5 mM imidazole) and lysed by ultrasonication. The cell lysate was then centrifuged at 2925 rcf for 1 h at 4 °C. The supernatant was loaded onto a pre-equilibrated Ni-nitrilotriacetic acid affinity column (Qiagen, Germany), and the column was washed with a buffer (50 mM sodium phosphate (pH 8.0), 300 mM sodium chloride, and 20 mM imidazole). The RidA protein was eluted with an elution buffer (50 mM sodium phosphate (pH 8.0), 300 mM sodium chloride, and 300 mM imidazole) and concentrated using a centrifugal filter (Amicon; Millipore, USA). The N-terminal polyhistidine tag of Pp-RidA was removed by digestion with thrombin, and the resulting protein solution was further loaded onto a Superdex 200 10/300 column (GE Healthcare, USA) pre-equilibrated with a buffer (20 mM Tris-HCl (pH 8.0) and 150 mM sodium chloride). The protein fractions were collected and concentrated to 12 mg/mL. The purity of the protein sample was assessed by sodium dodecyl sulfate-polyacrylamide gel electrophoresis.

2.2. Crystallization and data collection

Initial crystallization conditions were explored using the sitting-drop vapor-diffusion method with a crystallization robot (mosquito; TTP Labtech, UK) on 96-well crystallization plates (Emerald Bio, USA). Commercially available crystallization screening kits such as MCSG I-IV (Microlytic; CalibreScientific, USA), SaltRx, and Index (Hampton Research, USA) were used for crystallization. Protein solution (200 nL) was mixed with the same volume of each reservoir solution, and equilibrated against 80 μL reservoir solution. Crystals were observed under several crystallization conditions in approximately 2 days, which were further optimized. Diffraction-quality crystals were obtained using a buffer consisting of 0.1 M Bis-Tris propane/HCl (pH 7), 1.1 M malonic acid, 0.15 M ammonium citrate tribasic, 0.072 M succinic acid, 0.18 M DL-malic acid, 0.24 M sodium acetate, 0.3 M sodium formate, and 0.1 M ammonium tartrate dibasic. A well-formed single crystal was selected and soaked into Paratone-N oil (Hampton Research, USA) for cryo-protection. X-ray diffraction data were collected at −173 °C on the BL5C beamline at Pohang Accelerator Laboratory (PAL; Pohang, Korea). The data set contains 200 images with an oscillation range of 1° per image. The data were indexed, integrated, and scaled using the HKL2000 program.

2.3. Structure determination and refinement

The phase of RidA was determined by the molecular replacement method using the MOLREP program [19] in the CCP4 program suite [20]. The structure of the PSPTO-PSP protein from *Pseudomonas syringae pv. tomato str. DC3000* (PDB code: 3K0T; sequence identity: 60%) [21] was used as a search model. Subsequently, the initial model was further built using Coot [22] and refined using REFMAC5 [23] and phenix.refine [24] from CCP4 [25] and Phenix [26], respectively. The model refinement was completed when R_{sym} and R_{free} values reached 15.6% and 16.4%, respectively. The quality of the final model was validated using MolProbity [27]. Atomic coordinates and structure factors for Pp-RidA have been deposited in the Protein Data Bank under accession code 6L8P. Multiple sequence alignment was executed and represented using Clustal Omega [28] and ESPript 3.0 [29], respectively. Structural figures in this paper were generated using PyMOL [30].

2.4. Analytical ultracentrifugation

Analytical ultracentrifugation (sedimentation velocity) was performed using ProteomeLab XL-A (Beckman Coulter). Samples were centrifuged at 42,000 rpm at 20 °C. Scan data were plotted as radius and residuals-signal at intervals of 10 min, and signals were detected at 280 nm. Data were analyzed and produced using SEDFIT and GUSSI software, respectively.

2.5. Molecular docking simulation

A model of imine as a substrate for Pp-RidA was built using Avogadro [31]. The geometry of the model structure was optimized to minimized energy values. The pdbqt file of Pp-RidA and its substrate compound was generated using AutoDockTools 1.5.6 [32]. Several residues forming the putative active site of Pp-RidA were designated as flexible residues for accurate docking simulation. A virtual grid box for docking calculation included the flexible residues, and values for its size and spacing were set to 20 × 20 × 20 Å and 1 Å, respectively. Other parameters for docking simulation were set to default values. Molecular docking calculation was performed using Autodock Vina [33]. A total of 15 different conformers were generated according to binding energy scores. The top-ranked conformer was selected as a docking model.

3. Results and discussion

3.1. Overall structure of Pp-RidA

The structure of Pp-RidA was determined at 1.6 Å resolution by the molecular replacement method. Data collection and refinement statistics for Pp-RidA are summarized in Table 1. Three molecules in the asymmetric unit cell constitute a trimeric form (Fig. 1A). Forty-six residues per molecule are involved in interactions with their neighboring molecules (Fig. 1B), which amounts to 37%, considering that each molecule consists of 126 residues. Such a plethora of interactions imply that Pp-RidA can maintain a trimeric form in solution as well. Indeed, our analytical ultracentrifugation analysis showed a peak at approximately 3.3 sedimentation coefficient position, corresponding to 43.8 kDa (Fig. 1C). This indicates that Pp-RidA exits as a trimer in solution (theoretical Mw of trimeric Pp-RidA = 40.5 kDa). In addition, we observed a large cavity in the center of a vertical axis formed by the assembly of the three molecules, each with a tiny cavity (Fig. 1D).

The monomer of Pp-RidA consists of two α-helices (α1-2: residues 46–64 and 85–95, respectively), three 3_{10}-helices (η1-3: residues 69–71, 82–84, and 112–114, respectively), six β-strands (β1-6: residues 3–6, 21–24, 27–34, 73–79, 102–107, and 117–124, respectively), and four loops (L1-4: residues 7–20, 35–45, 65–68, and 96–101, respectively) (Fig. 1E). The β-strands, except for β5, form an antiparallel β-sheet. In the trimeric form of Pp-RidA, the convergence of these β-sheets results in a central β-barrel, which was surrounded by six α-helices. This structural feature is shared among other RidA proteins as well as Pp-RidA. In addition, structural superimposition revealed that the three molecules do not show significant structural differences, exhibiting root-mean-square-deviation (RMSD) values of 0.19–0.27 Å for 120 Cα atoms (Fig. 1F).

3.2. Malonate-binding site of Pp-RidA

We found a residual electron density map located in the interface between two subunits. A total of three residual electron density maps were identified. Malonate ions accurately fit into the electron density maps. Since the crystallization solution contained 1.1 M malonic acid, it is reasonable that a model corresponding to the map should be built with malonate. Interestingly, the position of malonate showed a remarkable spatial arrangement in terms of interactions with adjacent residues. Two oxygen atoms in the carboxyl group of malonate electrostatically interact with two nitrogen atoms in the guanidino group of the Arg103 residue on the β5-strand in a neighboring subunit (Fig. 2A). In addition, the β5-strand in the neighboring subunit was located at the end of the β-sheet. Hence, it is assumed that the multimeric form of Pp-RidA is an essential prerequisite for its substrate binding for catalysis.

We also found that malonate is surrounded by hydrophobic residues such as Val15, Tyr18, Gly32, Leu34, Phe85, Ala104, Ala105, and Pro112 (Fig. 2B). Strikingly, the L1 loop containing Val15 and Tyr18 appears to occlude access of the outer solvent to the malonate-bound site by covering the binding site (Fig. 2A). It may seem unfavorable that malonate with two hydrophilic carboxyl groups is positioned at the hydrophobic binding site. However, such a binding site can constitute a suitable environment, considering that a natural imine intermediate originating from threonine or serine retains a hydrophobic moiety such as a carbon chain.

Table 1
Data collection and refinement statistics of Pp-RidA.

Data collection	
X-ray source	BL-5C beamline
Wavelength (Å)	1.00000
Space group	$P2_12_12_1$
Unit cell parameter *a*, *b*, *c* (Å)	$a = 67.28$, $b = 71.14$, $c = 108.48$
Total reflections	479619
Unique reflections[a]	69280 (3385)
Multiplicity[a]	6.9 (7.4)
Completeness (%)[a]	100 (100)
Mean $I/\sigma(I)$[a]	36.6 (6.9)
R_{merge} (%)[a,b]	10.6 (48.6)
Resolution range (Å)[a]	50.00–1.60 (1.63-1.60)
Refinement	
Resolution range (Å)	42.24-1.60 (1.64-1.60)
No. of reflections of working set[a]	69200 (4684)
No. of reflections of test set[a]	2011 (138)
R_{work} (%)	14.8
R_{free} (%)	16.4
Ramachandran plot:	
favored/outliers (%)	99.2/0.0
Rotamer outliers (%)	0.0
RMSD bonds (Å)/angles (°)	0.012/1.135

[a] Values for the outermost resolution shell in parentheses.
[b] $R_{merge} = \Sigma_h \Sigma_i |I(h)_i - <I(h)>| / \Sigma_h \Sigma_i I(h)_i$, where $I(h)$ is the observed intensity of reflection h, and $<I(h)>$ is the average intensity obtained from multiple measurements.

3.3. Structural comparison with homologues

Several structures of the RidA proteins from not only mesophilic bacteria including *E. coli* (Ec-RidA; PDB code: 1QU9) [12] and *B. subtilis* (Bs-RidA; PDB code: 1QD9) [16], but also thermophilic and hyperthermophilic bacteria such as *H. thermocellum* (Ht-RidA; PDB code: 1XRG) and *S. tokodaii* (St-RidA; PDB code: 1X25) [17] have been determined thus far. To identify structural differences between Pp-RidA and its homologues, we compared their amino acid sequences and structures. Based on sequence alignment analysis and site-directed mutagenesis, it has been previously reported that the Tyr17, Arg105, and Glu120 residues of the RidA protein from *S. enterica* (Se-RidA) are critical to its enzymatic activity, suggesting that they are the key residues in the active site [1]. Therefore, the amino acid sequence of Pp-RidA was compared to that of homologues, including Se-RidA, to infer the active site residues of Pp-RidA [Fig. 3A]. The Tyr18, Arg103, and Glu118 residues of Pp-RidA are well conserved sequentially, which are also part of residues forming the malonate-binding site [Fig. 2A]. Interestingly, we found that Thr17 and Gly35 of Pp-RidA correspond to proline positions in other homologues [Fig. 3A]. A relatively less proline content has been observed in numerous cold-adapted proteins [34–36]. This can be interpreted as an evolutionary strategy to mitigate the risk of misfolding that could result from proline isomerization [37].

To gain insight into factors contributing to cold-adaptability of Pp-RidA, we also compared the structure of Pp-RidA with those of homologues such as mesophiles [Fig. 3B] and thermophiles [Fig. 3C]. Comparative analysis revealed that they share a common architecture [Fig. 3B–C]. RMSD values between Pp-RidA and the mesophilic homologues (Ec-RidA and Bs-RidA) are 1.2–1.4 Å for 120 Cα atoms, and those between Pp-RidA and the thermophile homologues (Ht-RidA and St-RidA) are 0.9–2.8 Å for 120–128 Cα atoms, respectively. These results suggest that Pp-RidA has the same enzymatic functions as the homologues, and factors contributing to its cold-adaptability may result from local structural variations.

We found that the L1 loop of Pp-RidA shows structural deviations among the homologues [Fig. 3D]. The L1 loop of Pp-RidA is positioned closer to the active site than the homologues [Fig. 3D], probably resulting in spatial restriction on substrate access. This

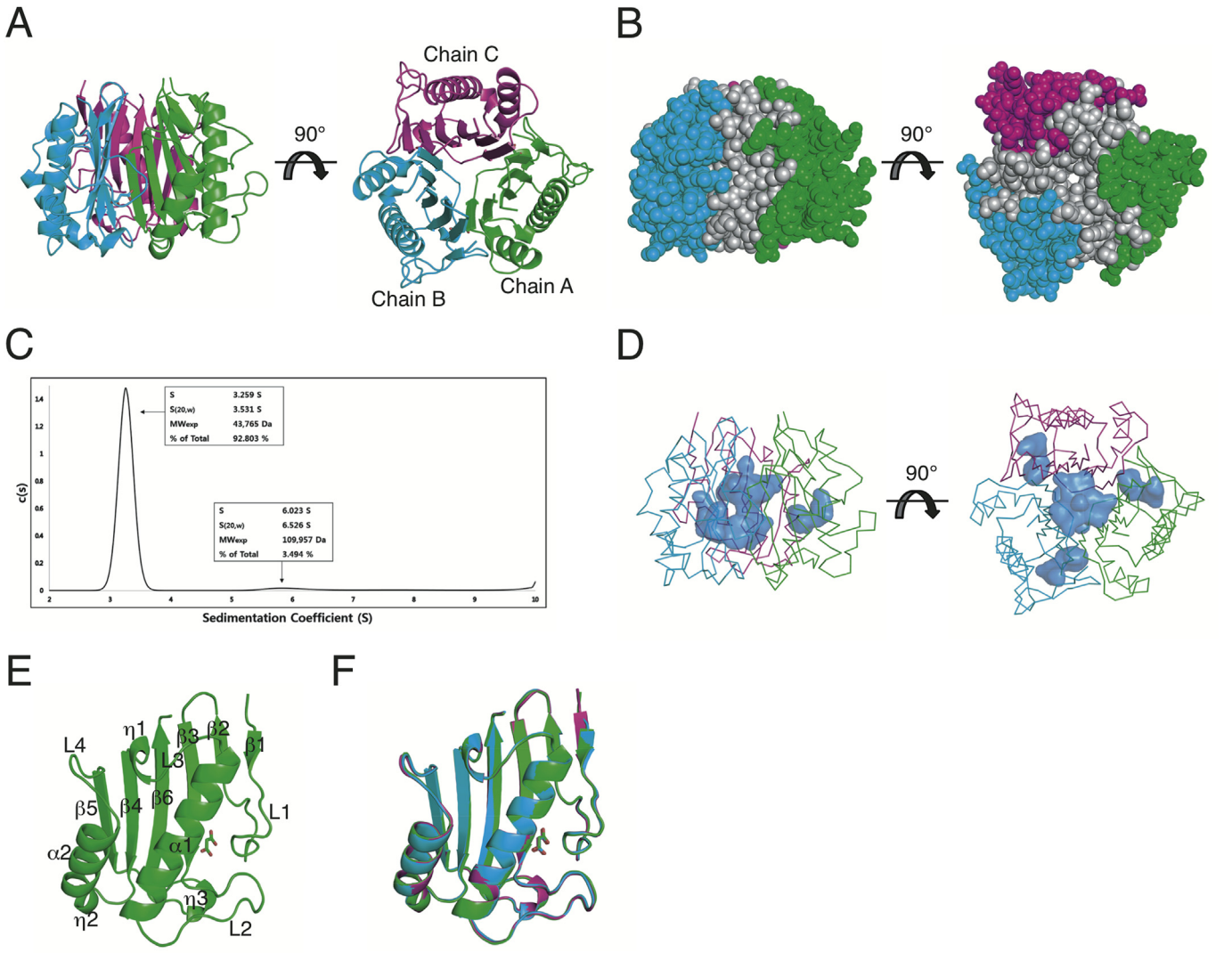

Fig. 1. Structure of Pp-RidA. (A) Overall structure of Pp-RidA in the asymmetric unit. Two different orientations of the 3D structure of trimeric Pp-RidA are depicted. (B) Interactions between the three subunits of Pp-RidA. The structure is represented as spheres and interface regions are colored grey. (C) Analytical ultracentrifugation profile of Pp-RidA. Data are plotted as sedimentation coefficient (x-axis) and sedimentation coefficient distribution (y-axis). (D) Cavities of Pp-RidA. The blue clumps indicate cavities including the one positioned in the center of the vertical axis. (E) The monomeric structure of Pp-RidA. (F) Superimposition of the three monomers of Pp-RidA. (For interpretation of the references to color in this figure legend, the reader is referred to the Web version of this article.)

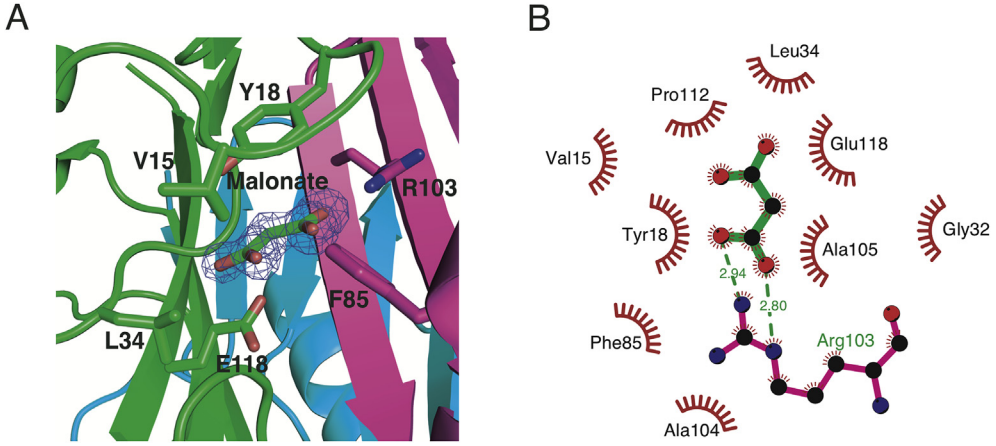

Fig. 2. Malonate-binding site of Pp-RidA. (A) Malonate and the residues interacting with it are represented as sticks. Part of interacting residues is omitted for clarity. The omit map (mF_o-DF_c) is colored blue and contoured at 3.0 σ. (B) Diagram of malonate interactions with adjacent residues. Blue and red circles, and green dashed lines indicate nitrogen and oxygen atoms, and hydrogen bonds, respectively. (For interpretation of the references to color in this figure legend, the reader is referred to the Web version of this article.)

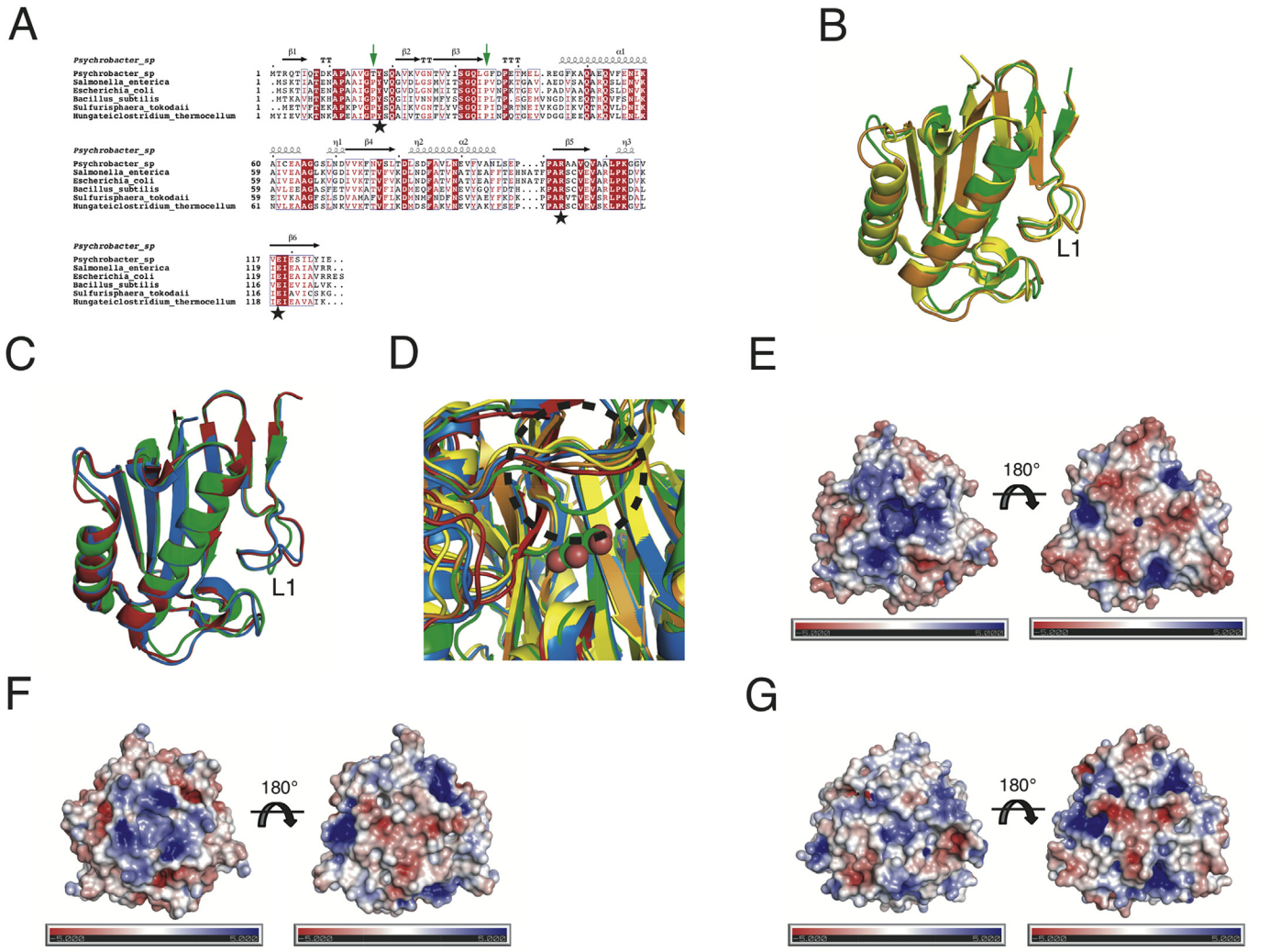

Fig. 3. Structural comparison of Pp-RidA with homologues. (A) Amino acid sequence alignment between Pp-RidA and homologues. The asterisks indicate conserved residues among Pp-RidA and homologues. The green arrows indicate substituted residues of Pp-RidA, corresponding to proline in homologues. (B) Overall structural comparison between Pp-RidA (green) and mesophilic homologues such as Ec-RidA (yellow) and Bs-RidA (orange). (C) Overall structural comparison between Pp-RidA (green) and thermophilic homologues such as Ht-RidA (blue) and St-RidA (red). (D) Zoomed-in view of the L1 loop region. The black dashed circle indicates a structural variation of the L1 loop. Malate is depicted as spheres. Color code is the same as in panels B and C. Surface electrostatic potential of Pp-RidA (E), Ec-RidA (F), and Ht-RidA (G). The scale bars range from −5 kT/e (red) to 5 kT/e (blue). (For interpretation of the references to color in this figure legend, the reader is referred to the Web version of this article.)

structural feature is commonly observed among the three monomers of Pp-RidA [Fig. 1E], implying that this spatial arrangement of the L1 loop of Pp-RidA, rather than a simple structural variation, may be associated with cold-adaptability. It is noteworthy that Tyr18 in the L1 loop is a putative key residue for catalysis. If L1 loops of the homologues should undergo conformational changes upon substrate binding to form the transition state geometry, the L1 loop including Tyr18 of Pp-RidA could contribute to reducing the activation energy for reaching the transition state. Contrary to those in the homologues, however, the L1 loop of Pp-RidA appears as if it limited access of the substrate to the active site. Such a spatial feature of the L1 loop possibly results in increased K_m values by rendering the substrate binding difficult. As a result, it is assumed that Pp-RidA adopts an enzymatic strategy to compensate for the increased K_m values by enhancing k_{cat} values.

In addition to the comparative analysis based on the superimposition, surface electrostatic potential of Pp-RidA and its homologues was analyzed. Ec-RidA and Ht-RidA were selected as comparison targets representing RidA from mesophilic and thermophilic bacteria, respectively. The central region of the vertical axis of Pp-RidA shows relatively strong positive charges [Fig. 3E] compared to those of the homologues [Fig. 3F and G], whereas negatively charged regions are more widely distributed on the opposite side of Pp-RidA [Fig. 3E]. In addition, positively charged residues are commonly distributed at the active site entrance. However, the entrance area of Pp-RidA is smaller than those of the homologues. Considering that Pp-RidA is from a psychrophile and water molecules move relatively inertly at low temperatures, such surface charge distributions of Pp-RidA possibly facilitate access of water molecules to the surface. The motion of water molecules on the surface may allow Pp-RidA to maintain protein dynamics required for its enzymatic function at low temperatures.

3.4. A possible substrate-binding mode

Enamine/imine intermediates are generally considered unstable [38]. Moreover, they can readily react with other molecules such as PLP, owing to the strong chemical reactivity [7,8]. Such a chemical property might have rendered the crystallization of RidA in complex with enamine/imine difficult. However, this complex structure

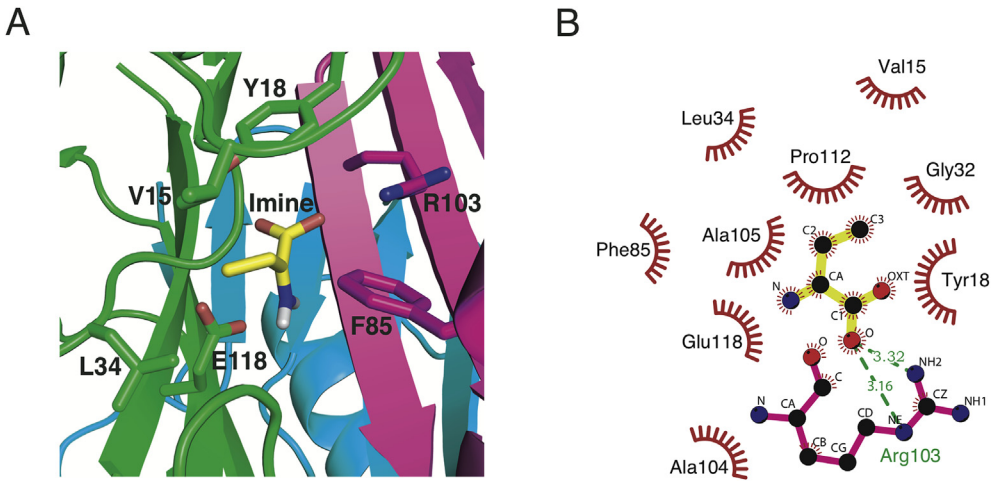

Fig. 4. Imine-binding mode predicted by molecular docking simulations. The imine conformer is colored yellow. The rest of the color code is the same as in Fig. 2A. (B) Diagram depicting the imine interactions with adjacent residues. (For interpretation of the references to color in this figure legend, the reader is referred to the Web version of this article.)

is indispensable in elucidating its catalytic mechanism at the molecular level. As an alternative, we performed molecular docking simulations of an imine molecule. For accurate simulations, key residues in the putative active site, such as Val15, Tyr18, Leu34, Phe85, Arg103, and Glu118 were designated as flexible residues.

The top-ranked docking simulation result is described in Fig. 4A. It showed that the conformer is positioned at the same site as malonate [Fig. 4A]. We found that the carboxyl group and protonated ketimine group form salt bridges with Arg103 and Glu118, respectively [Fig. 4B]. In addition, the alkyl group interacts with the neighboring hydrophobic residues such as Val15, Tyr18, Leu34, and Phe85 [Fig. 4B]. It appears reasonable that the two charged residues and a group of hydrophobic residues are appropriately assigned to the putative active site, taking into account that enamine/imine intermediates have an alkyl group consisting of at least one carbon. Such interactions probably contribute to thermodynamically stabilizing the reactive intermediate by facilitating the formation of geometry for catalysis. Accordingly, our docking result provides structural insight into the substrate-binding mode for the catalytic reaction of Pp-RidA.

Funding

This work was supported by a grant from Korea Polar Research Institute (grant number PE19210) and a grant from the Korea Healthcare Technology R&D Project, Ministry of Health & Welfare, Republic of Korea (HI17C0155).

Acknowledgements

The authors thank the BL5C beamline manager at PAL for helping the data collection and the Park's lab members for helpful discussion.

Transparency document

Transparency document related to this article can be found online at https://doi.org/10.1016/j.bbrc.2019.11.139.

References

[1] J.A. Lambrecht, J.M. Flynn, D.M. Downs, Conserved YjgF protein family deaminates reactive enamine/imine intermediates of pyridoxal 5'-phosphate (PLP)-dependent enzyme reactions, J. Biol. Chem. 287 (2012) 3454–3461.
[2] T.D. Niehaus, S. Gerdes, K. Hodge-Hanson, A. Zhukov, A.J. Cooper, M. ElBadawi-Sidhu, O. Fiehn, D.M. Downs, A.D. Hanson, Genomic and experimental evidence for multiple metabolic functions in the RidA/YjgF/YER057c/UK114 (Rid) protein family, BMC Genomics 16 (2015) 382.
[3] K.M. Hodge-Hanson, D.M. Downs, Members of the Rid protein family have broad imine deaminase activity and can accelerate the *Pseudomonas aeruginosa* D-arginine dehydrogenase (DauA) reaction in vitro, PLoS One 12 (2017), e0185544.
[4] J.A. Lambrecht, B.A. Browne, D.M. Downs, Members of the YjgF/YER057c/UK114 family of proteins inhibit phosphoribosylamine synthesis in vitro, J. Biol. Chem. 285 (2010) 34401–34407.
[5] J.A. Lambrecht, G.E. Schmitz, D.M. Downs, RidA proteins prevent metabolic damage inflicted by PLP-dependent dehydratases in all domains of life, mBio 4 (2013) e00033-13.
[6] D.C. Ernst, D.M. Downs, 2-aminoacrylate stress induces a context-dependent glycine requirement in RidA strains of *Salmonella enterica*, J. Bacteriol. 198 (2015) 536–543.
[7] H. Ueno, J.J. Likos, D.E. Metzler, Chemistry of the inactivation of cytosolic aspartate aminotransferase by serine O-sulfate, Biochemistry 21 (1982) 4387–4393.
[8] J.J. Likos, H. Ueno, R.W. Feldhaus, D.E. Metzler, A novel reaction of the coenzyme of glutamate decarboxylase with L-serine O-sulfate, Biochemistry 21 (1982) 4377–4386.
[9] D.M. Downs, D.C. Ernst, From microbiology to cancer biology: the Rid protein family prevents cellular damage caused by endogenously generated reactive nitrogen species, Mol. Microbiol. 96 (2015) 211–219.
[10] R. Morishita, A. Kawagoshi, T. Sawasaki, K. Madin, T. Ogasawara, T. Oka, Y. Endo, Ribonuclease activity of rat liver perchloric acid-soluble protein, a potent inhibitor of protein synthesis, J. Biol. Chem. 274 (1999) 20688–20692.
[11] A. Müller, S. Langklotz, N. Lupilova, K. Kuhlmann, J.E. Bandow, L.I. Leichert, Activation of RidA chaperone function by N-chlorination, Nat. Commun. 5 (2014) 5804.
[12] K. Volz, A test case for structure-based functional assignment: the 1.2 Å crystal structure of the yjgF gene product from Escherichia coli, Protein Sci. 8 (1999) 2428–2437.
[13] L. Parsons, N. Bonander, E. Eisenstein, M. Gilson, V. Kairys, J. Orban, Solution structure and functional ligand screening of HI0719, a highly conserved protein from bacteria to humans in the YjgF/YER057c/UK114 family, Biochemistry 42 (2003) 80–89.
[14] P. Juneja, F. Hubrich, K. Diederichs, W. Welte, J.N. Andexer, Mechanistic implications for the chorismatase FkbO based on the crystal structure, J. Mol. Biol. 426 (2014) 105–115.
[15] K.G. Thakur, T. Praveena, B. Gopal, *Mycobacterium tuberculosis* Rv2704 is a member of the YjgF/YER057c/UK114 family, Proteins 78 (2010) 773–778.
[16] S. Sinha, P. Rappu, S.C. Lange, P. Mäntsälä, H. Zalkin, J.L. Smith, Crystal structure of *Bacillus subtilis* YabJ, a purine regulatory protein and member of the highly conserved YjgF family, Proc. Natl. Acad. Sci. U.S.A. 96 (1999) 13074–13079.
[17] T. Miyakawa, W.C. Lee, K. Hatano, Y. Sawano, K. Miyazono, K. Nagata, M. Tanokura, Crystal structure of the YjgF/YER057c/UK114 family protein from the hyperthermophilic archaeon *Sulfolobus tokodaii* strain 7, Proteins 62 (2006) 557–561.
[18] H.Y. Koh, H. Park, J.H. Lee, S.J. Han, Y.C. Sohn, S.G. Lee, Proteomic and transcriptomic investigations on cold-responsive properties of the psychrophilic Antarctic bacterium *Psychrobacter* sp. PAMC 21119 at subzero temperatures, Environ. Microbiol. 19 (2017) 628–644.
[19] A. Vagin, A. Teplyakov, Molecular replacement with MOLREP, Acta Crystallogr. Sect. D Biol. Crystallogr. 66 (2010) 22–25.

[20] M.D. Winn, C.C. Ballard, K.D. Cowtan, E.J. Dodson, P. Emsley, P.R. Evans, R.M. Keegan, E.B. Krissinel, A.G. Leslie, A. McCoy, S.J. McNicholas, G.N. Murshudov, N.S. Pannu, E.A. Potterton, R.J. Read, A. Vagin, K.S. Wilson, Overview of the CCP4 suite and current developments, Acta Crystallogr. Sect. D Biol. Crystallogr. 67 (2011) 235–242.
[21] H.M. Zhang, Y. Gao, M. Li, W.R. Chang, Crystal structure of the PSPTO-PSP protein from *Pseudomonas syringae pv. tomato str. DC3000* in complex with D-glucose, Biochem. Biophys. Res. Commun. 397 (2010) 82–86.
[22] P. Emsley, K. Cowtan, Coot: model-building tools for molecular graphics, Acta Crystallogr. Sect. D Biol. Crystallogr. 60 (2004) 2126–2132.
[23] G.N. Murshudov, P. Skubák, A.A. Lebedev, N.S. Pannu, R.A. Steiner, R.A. Nicholls, M.D. Winn, F. Long, A.A. Vagin, REFMAC5 for the refinement of macromolecular crystal structures, Acta Crystallogr. Sect. D Biol. Crystallogr. 67 (2011) 355–367.
[24] P.V. Afonine, R.W. Grosse-Kunstleve, N. Echols, J.J. Headd, N.W. Moriarty, M. Mustyakimov, T.C. Terwilliger, A. Urzhumtsev, P.H. Zwart, P.D. Adams, Towards automated crystallographic structure refinement with phenix.refine, Acta Crystallogr. Sect. D Biol. Crystallogr. 68 (2012) 352–367.
[25] M.D. Winn, C.C. Ballard, K.D. Cowtan, E.J. Dodson, P. Emsley, P.R. Evans, R.M. Keegan, E.B. Krissinel, A.G. Leslie, A. McCoy, S.J. McNicholas, G.N. Murshudov, N.S. Pannu, E.A. Potterton, R.J. Read, A. Vagin, K.S. Wilson, Overview of the CCP4 suite and current developments, Acta Crystallogr. Sect. D Biol. Crystallogr. 67 (2011) 235–242.
[26] P.D. Adams, P.V. Afonine, G. Bunkóczi, V.B. Chen, I.W. Davis, J.J. Echols, L.W. Headd, L.W. Hung, G.L. Kapral, R.W. Grosse-Kunstleve, A.J. McCoy, N.W. Moriarty, R. Oeffner, R.J. Read, D.C. Richardson, J.S. Richardson, T.C. Terwilliger, P.H. Zwart, PHENIX: a comprehensive Python-based system for macromolecular structure solution, Acta Crystallogr. Sect. D Biol. Crystallogr. 66 (2010) 213–221.
[27] V.B. Chen, W.B. Arendall, J.J. Headd, D.A. Keedy, R.M. Immormino, G.J. Kapral, L.W. Murray, J.S. Richardson, D.C. Richardson, MolProbity: all-atom structure validation for macromolecular crystallography, Acta Crystallogr. Sect. D Biol. Crystallogr. 66 (2010) 12–21.
[28] F. Sievers, A. Wilm, D. Dineen, T.J. Gibson, K. Karplus, W. Li, R. Lopez, H. McWilliam, M. Remmert, J. Söding, J.D. Thompson, D.G. Higgins, Fast, scalable generation of high-quality protein multiple sequence alignments using clustal omega, Mol. Syst. Biol. 7 (2007) 1–6.
[29] X. Robert, P. Gouet, Deciphering key features in protein structures with the new ENDscript server, Nucleic Acids Res. 42 (2014) 320–324.
[30] The PyMOL molecular graphics system, Version 1.7.4, Schrödinger, LLC, Available online, http://www.pymol.org.
[31] M.D. Hanwell, D.E. Curtis, D.C. Lonie, T. Vandermeersch, E. Zurek, G.R. Hutchison, Avogadro: an advanced semantic chemical editor, visualization, and analysis platform, J. Cheminf. 4 (2012) 17.
[32] G.M. Morris, R. Huey, W. Lindstrom, M.F. Sanner, R.K. Belew, D.S. Goodsell, A.J. Olson, AutoDock4 and AutoDockTools4: automated docking with selective receptor flexibility, J. Comput. Chem. 30 (2009) 2785–2791.
[33] O. Trott, A.J. Olson, AutoDock Vina: improving the speed and accuracy of docking with a new scoring function, efficient optimization and multithreading, J. Comput. Chem. 31 (2010) 455–461.
[34] G. Feller, C. Gerday, Psychrophilic enzymes: hot topics in cold adaptation, Nat. Rev. Microbiol. 1 (2003) 200–208.
[35] G. Feller, Protein stability and enzyme activity at extreme biological temperatures, J. Phys. Condens. Matter 22 (2010) 323101.
[36] K.S. Siddiqui, R. Cavicchioli, Cold-adapted enzymes, Annu. Rev. Biochem. 75 (2006) 403–433.
[37] G. Feller, Psychrophilic enzymes: from folding to function and biotechnology, Scientifica (Cairo) 2013 (2013) 512840.
[38] A.J. Borchert, D.C. Ernst, D.M. Downs, Reactive enamines and imines *in vivo*: lessons from RidA paradigm, Trends Biochem. Sci. 44 (2019) 849–860.